ADVANCED OPTICAL MATERIALS
www.advopticalmat.de

Methylammonium Lead Tribromide Single Crystal Detectors towards Robust Gamma-Ray Photon Sensing

*Jeremy T. Tisdale, Michael Yoho, Hsinhan Tsai, Shreetu Shrestha, Kasun Fernando, Jon K. Baldwin, Sergei Tretiak, Duc Vo, and Wanyi Nie**

In recent years, hybrid perovskite single crystalline solid-state detectors have shown promise in γ-ray spectroscopy. Here, the γ-ray photon induced electrical pulses are investigated, which are produced by perovskite solid-state detectors made with the commonly used methylammonium lead tribromide crystals with chlorine incorporation. Under low electric field detector operation, slow pulses generated by γ-rays with average rise times of 65 µs are observed, which decreases to 20 µs when a higher electrical field of 500 V cm^{-1} is applied. However, the baseline becomes noisy quickly, which prevents collection of clean pulses for spectra construction. Further, by systematically measuring the temperature dependence and current–voltage characteristics, such instability is attributed to the local ion migration under electrical field creating a fluctuating dark noise, which presents a major challenge in perovskite γ-ray detector technologies. It is demonstrated that cycling the bias between positive and negative polarity can stabilize the detector, allowing for longer periods of pulse accumulation for generating energy resolved spectra with resolutions of ≈35% at 59.6 keV and ≈25% at 662 keV at room temperature. The study indicates that the main limiting factors of perovskite-based γ-ray detectors are slow rise times and bias instability. These challenges must be properly addressed to achieve reproducible, high-resolution γ-ray detection.

1. Introduction

In the last decade, organo-metallic halide perovskites (OMHPs) have quickly excelled in the realm of optoelectronics. For photovoltaics, perovskite solar cells have already exceeded 23% in power conversion efficiency in a short development period.[1–4] OMHPs have also become popular in many other optoelectronic applications, such as light-emitting diodes,[5,6] photodetectors,[7,8] and lasing applications.[9] Properties such as tunable band gaps,[10,11] low trap state densities,[12] and long carrier diffusion lengths make OMHPs a desirable material for a wide range of optoelectronic applications, as well as being a focus for other semiconducting device applications.[13,14]

These fascinating optoelectronic properties have recently sparked a new interest for applications of OMHPs for high-energy radiation detectors, which are considered as a critical technology in many fields, including nuclear safeguards, nuclear forensics, and astrophysics. Notably, current solid-state detector technologies using classical semiconductors have many challenges that must be overcome for wide spread development. For example, Cadmium Zinc Telluride (CZT) is a commercial γ-ray detection semiconductor achieving reasonable resolution (≈2% at 662 keV) at room temperature. However, the complicated and costly high-quality crystal growth for this semiconductor fabrication prohibits its broad adaptation. Another example of a more cost-effective semiconductor is high purity Germanium, (HPGe) which achieves an impressive resolution, (≈0.2% at 662 keV) albeit under operation at liquid nitrogen temperatures.[15] Thus, achieving cost efficient, robust high resolution detection at ambient conditions has been a long-time aim for semiconductor γ-ray detectors. In this arena, lead-halide based perovskites have been proposed as a new generation semiconductors in γ -spectroscopy for its low-cost solution process and simple crystal growth for room temperature detectors.[16–18] The incorporation of high-Z elements (i.e., Pb) underscores the opportunity for enhanced photoelectric interaction probability. Large band gaps and high resistivities are also essential for highly sensitive operation in the resistive mode.[19] Moreover, the long carrier lifetime and decent ambipolar mobility give great potential for single photon counting and pulse mode radiation sensing.[15]

Previous reports have shown promising proof-of-principle results for the application of perovskites as ionizing radiation

Dr. J. T. Tisdale, Dr. H. Tsai, Dr. S. Shrestha, Dr. K. Fernando, J. K. Baldwin, Dr. S. Tretiak, Dr. W. Nie
Center for Integrated Nanotechnologies (CINT)
Materials Physics and Applications Division
Los Alamos National Laboratory
Los Alamos, NM 87545, USA
E-mail: Wanyi@lanl.gov
Dr. M. Yoho, Dr. D. Vo
Safeguards Science and Technology (NEN-1)
Nuclear Engineering and Nonproliferation Division
Los Alamos National Laboratory
Los Alamos, NM 87545, USA
Dr. S. Tretiak
Physics and Chemistry of Materials Group (T-1)
Theoretical Division
Los Alamos National Laboratory
Los Alamos, NM 87545, USA
The ORCID identification number(s) for the author(s) of this article can be found under https://doi.org/10.1002/adom.202000233.

DOI: 10.1002/adom.202000233

detectors. For example, excellent response to charged particles (α-particles) was reported with devices based on hybrid and non-hybrid perovskites, methylammonium lead tribromide ($MAPbBr_3$), and cesium lead tribromide ($CsPbBr_3$), respectively.[20–22] High X-ray detection sensitivity has been shown in recent years with detectors based on methylammonium lead triidode ($MAPbI_3$) and $MAPbBr_3$ systems.[17,23,24] Moreover, high energy γ-ray detectors were also reported with hybrid and non-hybrid lead-based perovskites. Some of the pioneer results in this new application include: $CsPbBr_3$ showing γ-ray spectra with a resolution of 3.8% at room temperature for a 662 keV ^{137}Cs source at room temperature;[16] $MAPbI_3$ showing γ-ray spectra with a resolution of 6.8% at a lower temperature of 2 °C for a 122 keV ^{57}Co source;[18] and $MAPbBr_{2.94}Cl_{0.06}$ showing γ-ray spectra with a typical resolution of 12% for a 662 keV ^{137}Cs at room temperature.[25] Although the above reports have shown quite significant progress towards high-resolution γ-ray detectors, the device working mechanisms and operational stability are not well understood. These are critical challenges to overcome towards attaining reproducible, efficient, and robust γ-ray sensing.

To understand the hybrid perovskite detector behaviors for room temperature γ-ray spectroscopy, we investigate in detail the γ-ray photon induced pulses and the detector bias stability. Briefly, we observe an unusually long rise time (≈60–70 µs averages) in the electrical pulses from the hybrid lead perovskite detector upon exposure to γ-ray single photon source under low electric fields of 50 V cm^{-1}. To gain deeper insight on these issues, we systematically investigate the rise times of the detectors as a function of bias voltages, γ-ray energies, and temperatures. All of these parameters are found to greatly influence the average rise times of the detectors. The rise times are improved to an average of 20 µs when using larger electric fields of 500 V cm^{-1} at room temperature and are further reduced to an average of 10 µs at 500 V cm^{-1} and reduced operational temperature (213 K). However, a large standard deviation is still present, indicating an inconsistent response over time. Moreover, the detector becomes unstable after just a few minutes of operation that prevents an efficient pulse collection to construct proper spectra. By studying the current voltage characteristics, we found that biasing the detectors at relatively high electric fields (up to 1000 V cm^{-1}) resulted in permanent hysteresis effects and an increase in dark current, which was detrimental to the detector operation. Finally, we show that constant switching of the polarity for the bias voltage to the detector every 30 to 60 s helps to maintain clean signals for pulse collection, where we demonstrate a photopeak from ^{241}Am γ-rays (59.6 keV) with a resolution of ≈30-35% and another photopeak from ^{137}Cs γ-rays (662 keV) with a resolution of ≈20%. Our study suggests that serious research efforts are urgently needed on material and device optimization to stabilize the electronic properties of hybrid perovskites subjected to high electrical fields, which are critical to fabricate robust, room temperature γ-ray detectors attaining high spectral resolution.

2. Results and Discussion

In this work, we focus on $MAPbBr_{2.85}Cl_{0.15}$ single crystals for high-energy γ-ray detection because of its reproducible large single crystal growth. **Figure 1**a shows a typical optical absorption spectrum of the 5 mol% Cl-doped $MAPbBr_3$ single crystal, which agrees well with previously reported literature data on the optical properties of the $MAPbBr_{3-x}Cl_x$ hybrid perovskite system.[26–28] Also, our previous work demonstrates the capability of growing these crystals with precise Cl-doping percentages.[29] The Figure 1a inset is a picture of multiple single crystals used for detector fabrication. These crystals were grown with a range of dimensions with areas of 16–50 mm^2 and thicknesses around 2 mm. The transparency of these crystals alludes to consistent, high-quality growth of $MAPbBr_{2.85}Cl_{0.15}$ single crystals. Our previous work demonstrates the capability of growing these crystals with precise Cl-doping percentages. Figure 1b shows the energy band diagram for the Cr/$MAPbBr_{2.85}Cl_{0.15}$/Cr device employed here for γ-ray detectors. This device structure was chosen on the basis of Ohmic Cr contacts showing negligible hysteresis and low dark current at the interface with $MAPbBr_3$ as suggested by previous literature.[25,30,31] The reasoning behind the choice of the resistive device structure, is explained by the instability in the signal-to-noise ratio as seen in Figure S1, Supporting Information in the $MAPbBr_{2.85}Cl_{0.15}$ system. We found that under constant high electric field operations that are required to efficiently collect the γ-ray ionized charges, the pulse signals from the $MAPbBr_{2.85}Cl_{0.15}$ devices were only stable for a few seconds before the noise level became too high to discern appreciable pulses. Therefore, the resistive device structure provides an opportunity to use a technique we term "voltage cycling" to stabilize the device. If the device becomes unstable at a positive polarity, it is switched to a negative polarity and a stable signal is achieved again. Thus, by switching back and forth between positive and negative polarity, we were able to continue counting radiation pulses for many hours. This is achieved while ion migration is still in a reversible state, similar to preconditioning effects that have been explored in photovoltaic applications, in regards to ion migration and mitigation of negative effects.[32–34] These devices remained stable for about two months (as judged by testing once a week for 2 h to check if pulses were still achievable) before the device failed to detect radiation pulses. Because the interfaces have the same contacts, the pulse shapes and amplitudes are similar in both polarities. Figure 1c shows a picture of the γ-ray detector device and the encapsulation method used to protect the crystal. Here, the device is sealed inside of a scintillation vial in an argon-filled glovebox to protect the crystal from environmental damages during testing. Wires are bonded to the crystal using a small amount of silver paste or carbon glue, and the device is then connected via the two wires coming out of the scintillation vial cap. Figure 1d shows the average current density–electrical field (J–E) characteristics from −500 to +500 V cm^{-1} for four different encapsulated Cr/$MAPbBr_{2.85}Cl_{0.15}$/Cr devices. The error bars represent the standard deviation over five separate detectors at each measured voltage showing that devices studied here have similar current-voltage characteristics. The average resistivity value for the five measured devices is calculated to be 0.257 ± 0.147 GΩ cm[17,30,31] Figures 1e,f show typical pulses analyzed from the response of our devices to γ-ray photons emitted from ^{241}Am and ^{137}Cs sources, respectively. Here, the pulses collected from the detector are the basic elements for energy resolved spectrum construction, where the amplitudes should

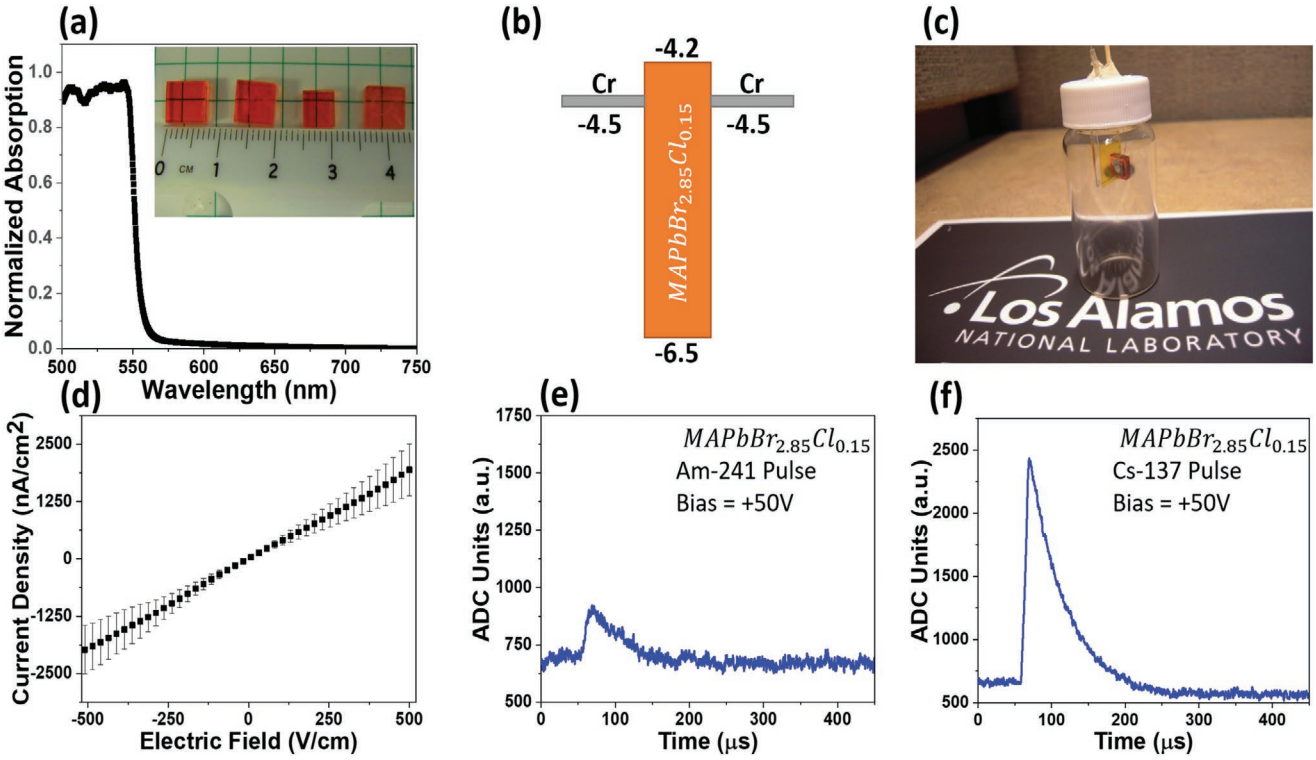

Figure 1. a) Average optical absorption spectrum for $MAPbBr_{2.85}Cl_{0.15}$ crystal. Inset shows high quality single crystals grown for this study and being used as-is for detectors. b) Band diagram of Cr/$MAPbBr_{2.85}Cl_{0.15}$/Cr device. c) Picture of full device encapsulated in argon using a scintillation vial. d) Average IV curve for Cr/$MAPbBr_{2.85}Cl_{0.15}$/Cr devices. e,f) Analyzed γ-ray pulses from Cr/$MAPbBr_{2.85}Cl_{0.15}$/Cr devices exposed to ^{241}Am and ^{137}Cs sources at room temperature, respectively.

change for various energies of γ-ray photons. For instance, in Figure 1e,f, the pulse height of the response to ^{137}Cs (662 keV) is much higher than that of ^{241}Am (59.6 keV), due to a significantly larger amount of charges ionized by the incoming high energy photons in the former case. However, we immediately notice an unusually slow rise time in the pulses generated by the perovskite detector under low bias at room temperature, which is not commonly seen in other semiconducting devices. Interestingly, we also observe different pulse shape from the same device under different sources. For example, the rise time is roughly 22 μs when exposed to ^{241}Am at 500 V cm^{-1}, while the rise time is roughly 15 μs when exposed to ^{137}Cs at 500 V cm^{-1}.

In order to gain a deeper understanding of the radiation detection properties of the $MAPbBr_{2.85}Cl_{0.15}$ hybrid perovskite, we further investigate the γ-ray induced pulses in the detector in greater details as summarized in **Figure 2**. Specifically, we extract the average rise times and plot them in histograms under various γ-ray energies and external applied electric fields. Rise time of the detectors is very important to understand, as this property directly relates to the resolution of the detector. A high-energy resolution comes from a fine distribution of high amplitude pulse events (called photo-electric effects).[15] Slower rise times allude to possible significant trapping/detrapping of charge carriers, especially with large deviations, making pulse collection challenging. Also, fast rise times are needed to be properly recorded by commercial electronics (i.e., multi-channel analyzers, charge sensitive preamplifiers, etc.), since we are counting single photon interactions. In Figure 2, the histograms represent extracted rise times from one device over 1000 pulses, to demonstrate the distribution of the detector signals over time in a short period (roughly 5–10 s to collect 1000 pulses). Figure 2a compares the average rise times and standard deviation (represented by error bars) of $MAPbBr_{2.85}Cl_{0.15}$ based detector to a standard commercial CZT crystal encased using the same resistive device structure. The CZT detector shows faster rise times with an increase in electric field, ranging from an average value of 8 μs down to 2 μs. Similar field dependence was observed in the perovskite devices. At a low electric field of 50 V cm^{-1}, the average rise times are first very slow at an average of 56–64 μs (positive/negative polarity), while it becomes drastically faster at a higher electric field of 300 V cm^{-1}, with an average value of 15–27 μs (positive/negative polarity). The long rise time in the hybrid perovskite-based detector was also observed in the literature under low bias.[30] At electric fields above 250 V cm^{-1}, the average rise times stabilize around 10–20 μs. This is expected alluding to the fact that the mobility of the charges is approaching a maximum at higher electric fields (≥ 300 V cm^{-1}).[35] At a maximum electric field of 500 V cm^{-1}, the average rise time is about 15 μs equally for both polarities. Above 500 V cm^{-1}, the noise level of the detector was too high to discern appreciable pulses in the signal because of large dark current. At low biases, the standard deviation is noticeable for both materials. For example, the CZT device showed an average rise time of 7 ± 2.4 μs at low fields and a more consistent response at 1.7 ± 0.3 μs when the field is

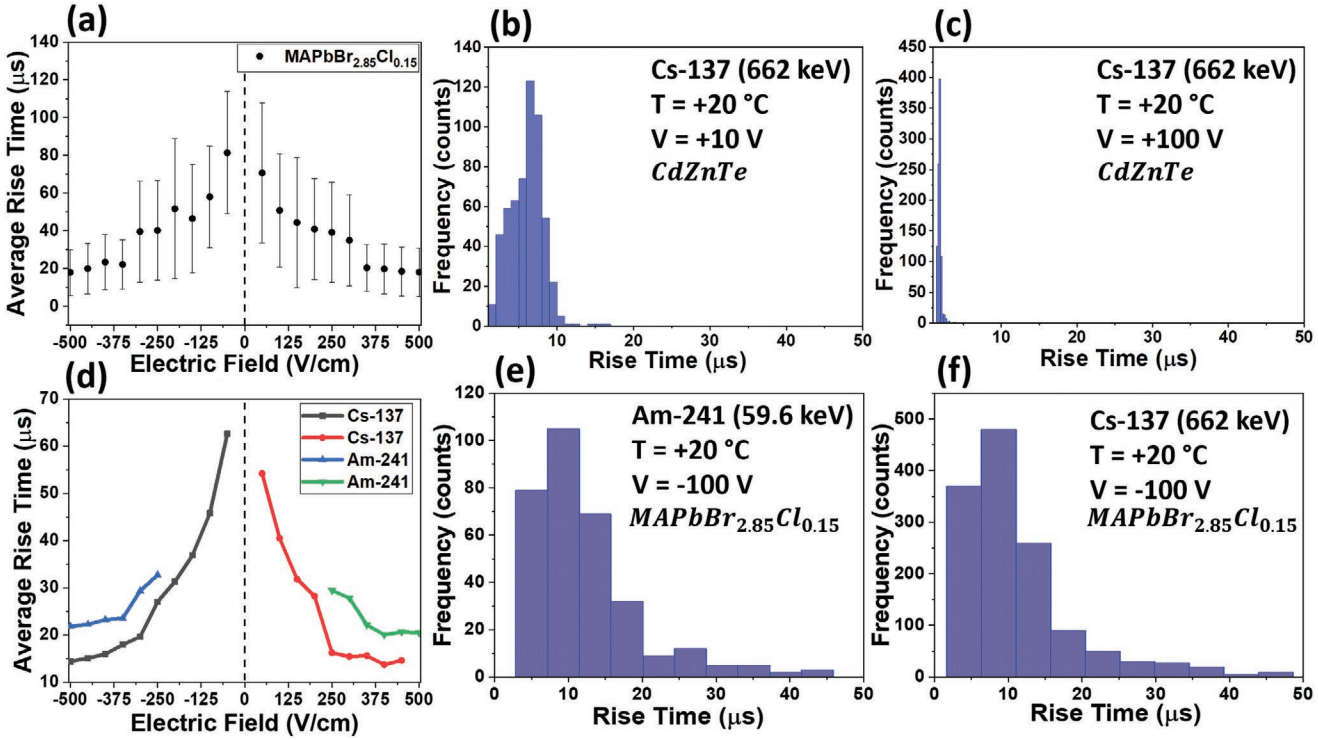

Figure 2. a) Average rise times for $MAPbBr_{2.85}Cl_{0.15}$ as compared to standard CZT device. (Error bars represent standard deviation.) b,c) Histograms of room temperature rise times for CZT device at +10 and +100 V, respectively. d) Bias dependent average rise times for devices when exposed to ^{241}Am and ^{137}Cs sources. e,f) Histograms of room temperature rise times at a bias voltage of −100 V for ^{241}Am and ^{137}Cs, respectively.

higher. On the other hand, the $MAPbBr_{2.85}Cl_{0.15}$ showed a much larger average value and standard deviation at 70.7 ± 37.2 μs. It still presented a much larger deviation in the rise times at 18.1 ± 12.8 μs at high field.

Figure 2d shows the rise time averages for the same detector under two different sources of γ-radiation, namely ^{137}Cs (662 keV) and ^{241}Am (59.6 keV). Interestingly, the average rise times of the detector in response to 662 keV γ-rays were faster than that under ^{241}Am sources. In Figure S2a, Supporting Information, we repeated similar measurements with a standard planar CZT detector for comparison. With the CZT detector, the difference in response between ^{137}Cs (662 keV) and ^{241}Am (59.6 keV) was negligible compared to the perovskite detectors, which shows that this phenomenon is more unique to the hybrid perovskite system. Note that in response to 59.6 keV γ-rays from ^{241}Am, below 250 V cm^{-1}, we were unable to observe any pulses above the noise floor. Figure 2e,f show the histograms for all pulses analyzed within the five second measurements, resulting in roughly 1000 pulses. As shown in Figure 2e, the rise times have a large standard deviation at low biases, where the pulses form in many different shapes and rise times, resulting in low resolution detection. Even at high electric fields, while the rise times of majority pulses fall into 10–20 μs range, we still observe an appreciable amount of counts up to 50 μs rise times. These data demonstrate a significant challenge for γ-ray spectroscopy using perovskite detectors made with $MAPbBr_{2.85}Cl_{0.15}$. The distribution of rise times (and pulse shapes) must be more consistent to provide reproducible, high-resolution spectra. Moreover, the device response changes as a function of γ-ray energy. Thus, calibrating the detector based on various energies of γ-rays becomes more difficult due to the non-uniform response. This shows that this material must be optimized to reduce the amount of slow rise times. In order to do so, slow rises must be reduced as much as possible by reducing the amounts of defects and mitigating ion migration, thereby removing inconsistencies via non-uniform electric fields. This can be done via compositional or device engineering.

Based on the understanding of classical γ-ray detectors, the large device distributions can be attributed to two origins: significantly different electron/hole transport, and large amounts of charge trapping/detrapping processes for one type of carrier, causing a non-uniform electric field throughout the detector.[19] We propose that both appear in our study due to different mechanisms including: 1) different energy photons deposit their energy differently across the crystal leading to non-uniform charge generation, 2) charge trapping–detrapping process slows down the pulse rise time, and 3) charge generated by low energy photons are more affected by trapping. Higher bias improves the pulse rise times; however, the large distribution problem remains, and the detectors become unstable in shorter periods of time.

Next, we examine the temperature dependence of the response of the γ-ray detectors. **Figure 3**a shows the average rise times of $MAPbBr_{2.85}Cl_{0.15}$ in response to ^{137}Cs as a function of temperature. Here, we observe a strong temperature dependence on the average rise times of the detectors. It is clear that reducing the temperature greatly improves the rise time of

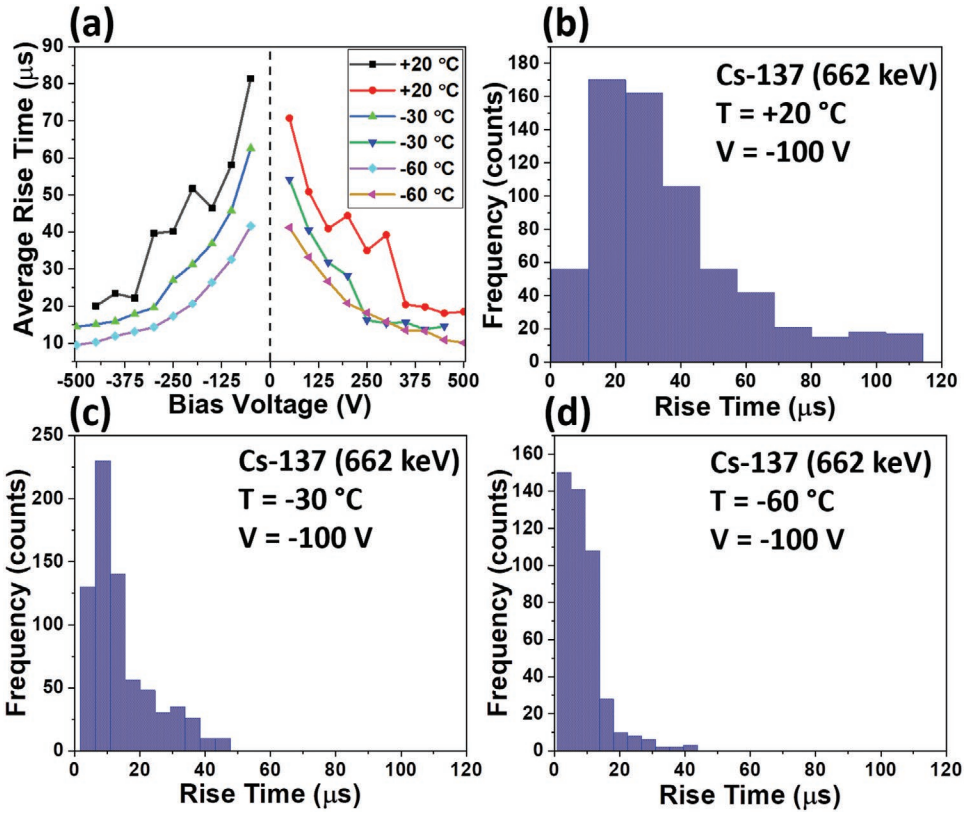

Figure 3. a) Temperature dependence of average rise times of Cr/$MAPbBr_{2.85}Cl_{0.15}$/Cr devices in response to ^{137}Cs γ-rays. b–d) Histograms for rise times at a bias voltage of −100 V, at +20 °C, −30 °C, and −60 °C, respectively.

the pulse signal. At 250 V cm^{-1}, the average rise time reduces from 40 μs at room temperature to 26 μs at −30 °C. Further decreasing the temperature improves the rise time even farther to 16 μs at −60 °C.

Figures 3b,c,d show the histograms for all of the analyzed pulses of the $MAPbBr_{2.85}Cl_{0.15}$ detector at room temperature, −30 and −60 °C, respectively. Note, the histograms here were taken on a different detector from the one measured in Figure 2, due to the large deviation from sample to sample existing in the hybrid perovskite detectors. However, the slow pulses and large distributions trend still holds for many devices tested. By comparing the three histograms of rise time distribution at different temperatures (all histograms were collected from one detector), two trends are clearly observed. The first trend shows that the mode (the most common value in a dataset) of the datasets significantly decreases with decreasing operational temperature. At +20 °, −30, and −60 °C the modes measured were around 20, 9, and 3 μs, respectively. The second trend implies that the distribution also reduces with decreasing temperature. At room temperature, we observe many slow pulses between 50 and 115 μs. These slow pulses are likely caused by thermal processes under ambient conditions, as well as significant trapping. However, the range of pulses drastically decreases with temperature, showing no pulses greater than 47 and 43 μs rise time at −30 and −60 °C, respectively. In Figure S2b, Supporting Information, we repeated the temperature dependent measurements for a standard CZT detector between 60 and 1000 V cm^{-1}. Here, we observe that the temperature dependence of the CZT detector is negligible as compared to the hybrid perovskite detector, where the rise time changes slightly at low electric fields from 60 to 100 V cm^{-1}. According to previous literature, such change corresponds to temperature dependent trapping effects.[36] On the other hand, in the perovskite system, the average rise times and pulse shape profiles change much more dramatically with temperature. This alludes to the fact that the large temperature dependence phenomenon is unique to the hybrid perovskite system. Therefore, we propose that this temperature dependence occurs due to slowing down ion migration and the freezing of shallow defects in the $MAPbBr_{2.85}Cl_{0.15}$ detectors at lower temperatures.

From these results we conclude that the rise time is very sensitive to the operating temperature, which reduces quite efficiently by a small drop in temperature. Lowering the temperature also helps to cut down on the amount of slow pulses. We do not expect such drastic change in the intrinsic carrier transport properties (i.e., mobility and lifetime) within the small temperature range (i.e., 293–210 K). The phase transition for $MAPbBr_3$ crystal occurs near 160 K which is also not the origin for a sharp decrease in rise time.[37–39] Combining the observation of voltage instability during detector operation (Figure 2 and Figure S1, Supporting Information) and the large temperature dependent rise time changes in Figure 3, we attribute the slow detector rise time to the ion migration induced charge trapping, which is greatly suppressed once the temperature is lowered.

A similar scope of phenomena was observed during the photovoltaic device operation, when the slow current transient

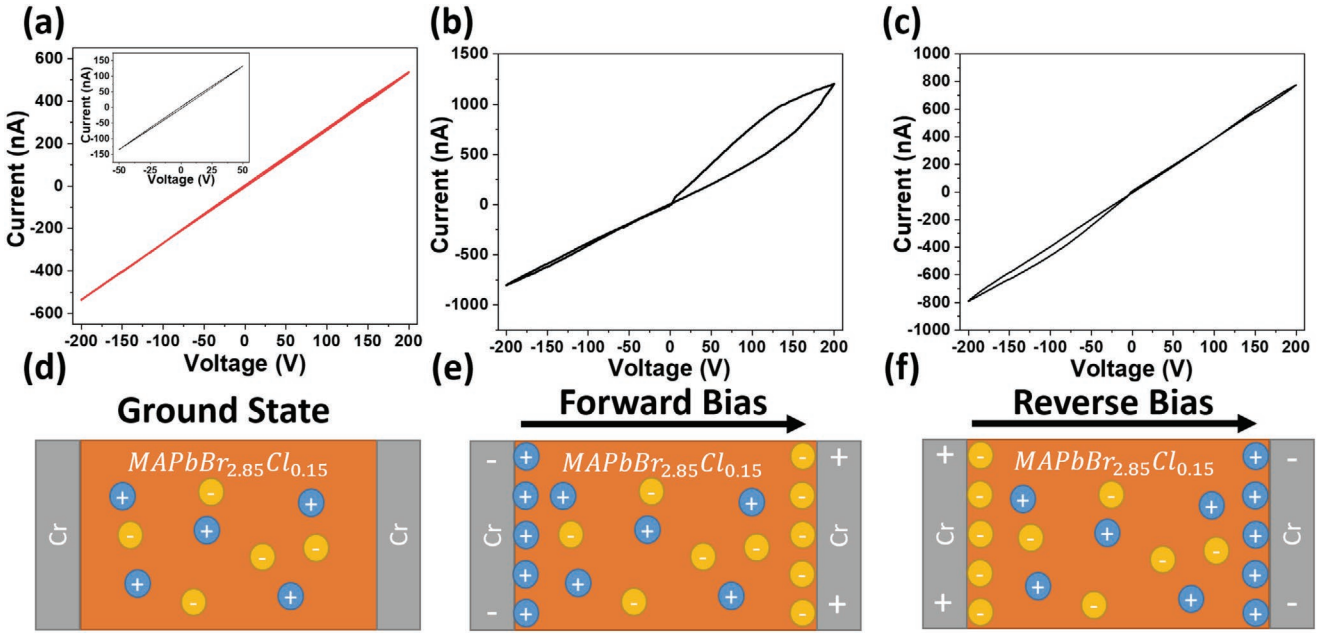

Figure 4. a) Dark *I–V* loop of fresh Cr/$MAPbBr_{2.85}Cl_{0.15}$/Cr device. b) *I–V* loop after long term biasing at voltages from +25–200 V in 25 V increments at 10 min each. (c) *I–V* loop after long term biasing at voltages from −25–200 V in 25 V increments at 10 min each. d–f) Schematic representation of mechanism, where + and − represent positive and negative charge and/or ions, respectively.

was identified to be detrimental to the device performance and was attributed to the ionic movement either locally or throughout the materials under bias.[40–43] It is understood that the dominant mechanism revealing this undesirable behavior is due to ion migration forming and releasing ionic charge build-up at device interfaces. In order to solve this problem in single crystalline hybrid perovskites, studies have shown that certain interfaces can cause hysteretic behavior due to interfacial recombination, low interfacial resistance, and chemical reactions at the interface forming metal-halide compounds between the semiconductor and electrode.[31,44] In the single crystal devices, similar issue may also exist. Therefore, we characterize the current–voltage curves and instability through monitoring hysteresis as a function of long-term, high voltage biasing on our detector in dark as summarized in **Figure 4**.

Figure 4a shows the *I–V* characteristics of a freshly made Cr/$MAPbBr_{2.85}Cl_{0.15}$/Cr device. It presents negligible hysteresis when scanned from −200 to +200 V (scan rate = 1 V s^{-1}), which is the operating bias range during γray detection. However, as discussed previously, there is a high level of instability under electric field for these hybrid perovskite detectors. To reproduce such phenomena, bias voltages were subsequently applied from 25 to 200 V in 25 V increments for 10 min each on this fresh device (current as a function of time and bias voltage is shown in Figure S3, Supporting Information). After each constant bias, the same *I–V* loop was measured following the scan protocol in Figure 4a to determine if any changes occurred in the dark current and hysteretic behavior of the device. (Figure S4, Supporting Information shows each *I–V* loop as a function of constant bias voltage.) Figure 4b,c show *I–V* loops for two different devices, two days after long-term biasing measurements. Here, not only do we show that hysteretic behavior is introduced to the device, (which was previously non-hysteretic) also we observe that the hysteresis is an irreversible effect when subjected to high voltage biasing for only a short time of roughly 10 min. We also measured capacitance of the devices after prolonged high voltage biasing to further confirm this trend. The capacitance of two separate devices were measured at a frequency of 100 kHz (notably, changing the frequency of the measurement had little to no effect in the range of 1000 Hz to 1 MHz.) Previous to long-term biasing of the devices, the capacitance of the first and second devices were 5.07 and 10.59 pF, respectively. These values were different due to size differences in the detectors. After biasing both detectors at 200 V, the capacitance values for the first and second devices increased to 8.52 pF (68% increase) and 11.79 pF (11% increase), respectively. Although increases in capacitance were relatively small, we observe that the electronic properties of $MAPbBr_{2.85}Cl_{0.15}$ clearly change under high bias operation, which is undesirable for high energy radiation detection.

This high-bias hysteresis effect is proposed to be the cause for high electric field instability of this hybrid perovskite system. Here, we note that the hysteresis only appears in the bias direction of which the negative charge collects at the interface. That is, when the device is biased, the Br^- ions drift towards the positively biased electrode, while the organic cations drift towards the negatively biased electrode. Therefore, as depicted in Figure 4e,f, when the device is biased in the forward direction, the Br^- ions drift to the right electrode, while the Br^- atoms drift towards the left electrode when the device is biased in the reverse direction. This alludes to the proposed mechanism, as depicted in Figure 4d–f. In previous reports, it has been shown that Br^- atoms can form complexes with metals such as Au.[44] However, this was found to be a reversible formation at low biases, important for optoelectronic processes, where the Cr/$MAPbBr_3$ interface did not show signs

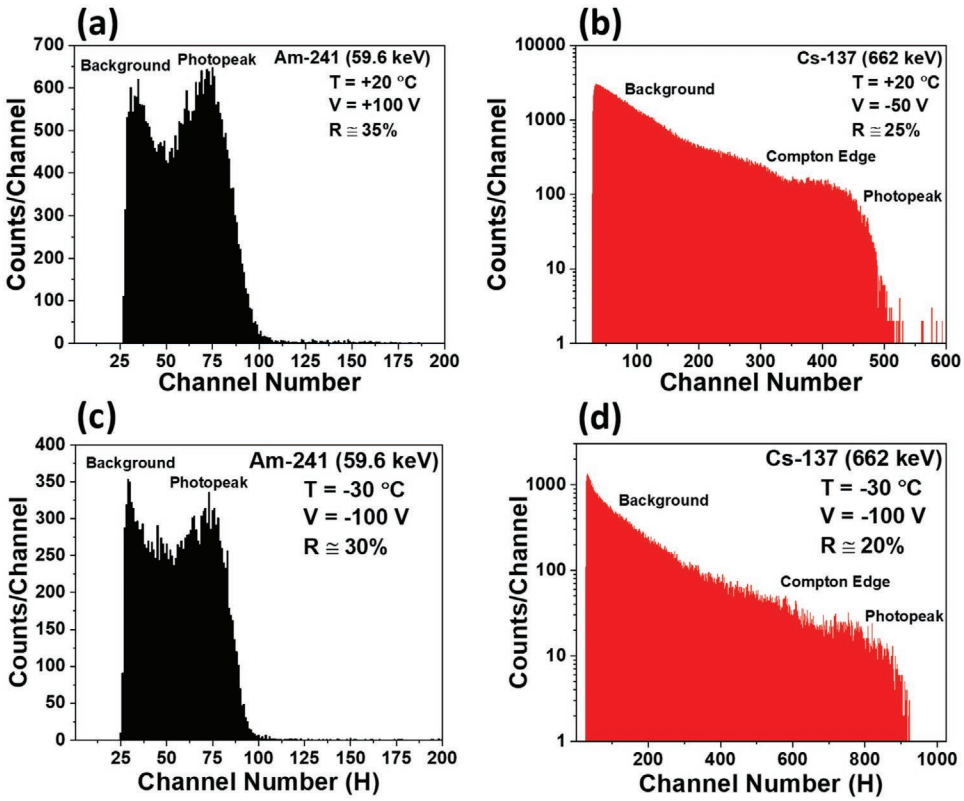

Figure 5. a,c) Energy spectra of ^{241}Am from Cr/$MAPbBr_{2.85}Cl_{0.15}$/Cr at room temperature and −30 °C, respectively. b,d) Energy spectra of ^{137}Cs from Cr/$MAPbBr_{2.85}Cl_{0.15}$/Cr at room temperature and −30 °C, respectively.

of hysteresis at lower voltages.[31] For high-energy γ-ray detection, where single photon induced pulses need to be collected, high electric fields are required for optimized charge collection efficiency and reduction of trapping to ensure high resolution signal. The fact that the hysteresis in the device is now permanent alludes to the possibility that either the charge or ion accumulation at the interface leads to a reaction that changes the properties of the interface, thereby changing the charge transfer processes at the interface.

Finally, when attempting to build the energy resolved spectrum, we count the pulses over an extended period of time as shown in **Figure 5**. At room temperature, we clearly identify the photopeak from ^{241}Am shown at channel number 75 using an electric field of about 500 V cm^{-1} in Figure 5a. Note, the spectra from the low energy 59.6 keV γ-rays were only collected at a larger electric field due to poor signal to noise ratio at lower electric fields. For the room temperature ^{137}Cs spectra, shown in Figure 5b, we observe a low-resolution photo-electric peak around channel number 425 due to low resolution the photopeak from 662 keV. This peak combined with the Pb escape peak at 587 keV, results in a very wide energy peak. Because of the device instability at large electric fields, we collected the spectra at half the electric field from the ^{241}Am spectra. Therefore, if we calibrate the energies from the photopeak of 59.6 keV at channel number 75 (Figure 5a), the photopeak from 662 keV should accurately be observed around channel number 425 (Figure 5b), confirming energy calibration between spectra. Typically the 662 keV photopeak position would be positioned around channel number 825, but the electric field was half the strength of the spectrum collected with the 59.6 keV source.

Figure 5c,d show the same energy spectra for ^{241}Am and ^{137}Cs at -30°C. Comparing the photopeak position of the different energies at the same electric field, 59.6 keV appears at the channel number 75. Based on this, for an equivalent electric field, the 662 keV should appear around channel number 825, confirming the spectra here as well. As discussed previously, a reduced temperature helps us to suppress the ion migration and freeze trapping in the detector and allows the device to remain stable at high electric fields about 5 min before becoming noisy in order to count for longer times. We were thus able to improve the resolution of the energy spectra by ≈5% at −30 °C. Here, we note that the low temperature significantly decreases the average rise times of the detector as shown from Figure 3. Also, the reduced temperature may reduce the dark current of the detector, thereby increasing the dark resistance of the detector. These enhanced properties should lead to an improvement in resolution of the detectors. However, as discussed above, problems like inconsistent pulse shapes and rise times still exist, and both lead to a poor pulse collection efficiency from these detectors even at reduced temperatures. These inconsistent pulse shapes possibly arise from phenomena such as trapping/detrapping of charge carriers, low efficiency for higher energy γ-rays interactions with atoms, imbalance of mobility between holes and electrons, and more. These issues lead to poor resolution, which is the reason that the photoelectric peak at 662 keV is not clearly defined.

Although the resolution of these detectors is relatively low to previously reported literature,[25] the low resolution spectra do agree with other reports that have presented similar resolution for other hybrid perovskite compositions.[35,45]

3. Conclusions

In conclusion, we have carried out an in-depth study on the operation of Cr/$MAPbBr_{2.85}Cl_{0.15}$/Cr single crystal devices for γ-ray spectroscopy. First, we observed an unusually slow rise time in the electrical pulses generated by the perovskite single crystal devices upon γ-ray photon exposure. Moreover, a large distribution in rise time over many pulses collected from the same device was also recorded. The energy of the γ-ray changed the response of the detector, with faster rise times at higher energies. Then, the average rise times were found to drastically reduce by over 75% when increasing the electric field strength from roughly 50 V cm^{-1} up to 500 V cm^{-1}, indicating the importance of operating at high electric fields. However, the detector quickly becomes unstable under constant high electrical field at one polarity. Third, we found the rise time was highly sensitive to the operating temperature, which led to the conclusion that the slow device response could originate from the trapping/detrapping of charge carriers coming from the field induced ionic movement. While low temperature and voltage cycling improved the stability of the detectors, the combined effects were not sufficient to achieve high resolution photo-electric peaks.

We attribute the low resolution and performance of these detectors to several factors including slow charge trapping and detrapping, ion migration and charge accumulation creating a variable, non-uniform electric field across the detector, and overall instability at high electric fields. Convolution of these problems in hybrid perovskite detectors results in poor signal to noise ratios and short counting time windows on the order of seconds to minutes that prevent the collection of high-resolution spectra. Therefore, these challenges must be fully resolved to achieve low-cost, hybrid perovskite solid state detectors with reproducible, high-resolution γ-ray spectroscopy at room temperature.

4. Experimental Section

Materials: N,N-Dimethylformamide (DMF, Sigma-Aldrich, anhydrous, 99.8%), $PbBr_2$ (Alfa Aesar, Puratonic, 99.998%), MABr (GreatCell Solar, ≥99%), MACl (Sigma-Aldrich, ≥98%), and Chromium metal (Kurt J. Lesker, 99.98–99.998%). The materials used for solution growth were used as-received.

Growth of OMHP Single Crystals and Device Fabrication: $MAPbBr_{2.85}Cl_{0.15}$ single crystals were grown using the inverse temperature crystallization (ITC) method.[46] $MAPbBr_{2.85}Cl_{0.15}$ single crystals were grown with 5%-doping of Cl based on replacement of Br in molar ratio of 1:0.85:0.15 M ($PbBr_2$:MABr:MACl). To prepare the growth solution, a mixture of $PbBr_2$, MABr, and MACl were dissolved in DMF to form the concentration of 1M. Here, high purity precursors were used, as compared to typical low purity precursors in literature, due to recent reports showing that higher purity precursors improves the quality of $MAPbBr_3$ single crystals.[20] The solution was placed under magnetic stirring at room temperature for 2 h to ensure full homogeneous dissolution of all precursors. Then the solution was filtered using 0.45 µm PTFE filters and separated into scintillation vials with 3 mL of solution each. The vials were placed in a silicone oil bath and slowly heated from 60 to 80 °C, at 5 °C per day. Full crystallization took place at 75–80 °C depending on vial placement, with an average crystal size of 5 × 5 × 2 mm or larger. After crystallization, the single crystals were dried with absorbent clean room paper and stored in a desiccator until device fabrication. For device fabrication, Cr was deposited via E-beam evaporation onto both sides of the single crystals with thicknesses of 70 nm each. Wires were attached using silver or carbon paste, and the devices were sealed in scintillation vials in an inert Argon atmosphere to protect from environmental effects.

Measurements Techniques: Absorption measurements were completed using a transmission mode spectrometer, due to the thickness and high absorption coefficient of the single crystals. Then the data was converted to absorption of the single crystal. Photoluminescence measurements were completed using a 405 nm laser with a spot size of one to two microns and a Pro EM 1024 spectrograph from Princeton instruments. *I*–*V* measurements were done using a Keithley 2450 sourcemeter and LabVIEW program. All I–V measurements used a scan rate of 1 V s^{-1} to keep a constant scan speed. The pulse processing chain for radiation measurements used two sets of processing. For all measurements we used a Keithley 6847 Picoampmeter/Voltage source for high voltage (HV) power, an Ortec 142 PC preamplifier with an Ortec 4002P preamp power supply, a low noise preamplifier filter (Stanford Research Systems) SR560, and a Tektronix PPO 4104 digital phosphor oscilloscope. A Pixie-Net from XIA was used to record individual pulses for rise time averages. We observed about 200 counts per second, and measured pulses for 5 s to eliminate noise from instability. Therefore, each measurement averaged about 1000 pulses during a stable period of the detector. For spectra collection, we used an Ortec Dspec-Pro MCA paired with Maestro v7.01 from Ortec. A TestEquity Model 115 temperature chamber was used for low temperature measurements.

Supporting Information

Supporting Information is available from the Wiley Online Library or from the author.

Acknowledgements

This work was supported by Laboratory Directed Research & Development (LDRD) funding from the LDRD Office at Los Alamos National Laboratory. Part of the work was performed at the Center of Integrated Nanotechnology (CINT) at Los Alamos National Laboratory.

Conflict of Interest

The authors declare no conflict of interest.

Keywords

gamma-ray spectroscopy, hybrid perovskites, ion migration, semiconductor detectors

Received: February 8, 2020
Revised: February 25, 2020
Published online: March 29, 2020

[1] Best Research-Cell Efficiencies, https://www.nrel.gov/pv/assets/pdfs/pv-efficiency-chart.20181221.pdf (accessed: August 2019).
[2] A. K. Jena, A. Kulkarni, T. Miyasaka, *Chem. Rev.* **2019**, *119*, 3036.

[3] W. Nie, H. Tsai, R. Asadpour, J.-C. Blancon, A. J. Neukirch, G. Gupta, J. J. Crochet, M. Chhowalla, S. Tretiak, M. A. Alam, H.-L. Wang, A. D. Mohite, *Science* **2015**, *347*, 522.
[4] H. Tsai, W. Nie, J.-C. Blancon, C. C. Stoumpos, R. Asadpour, B. Harutyunyan, A. J. Neukirch, R. Verduzco, J. J. Crochet, S. Tretiak, L. Pedesseau, J. Even, M. A. Alam, G. Gupta, J. Lou, P. M. Ajayan, M. J. Bedzyk, M. G. Kanatzidis, A. D. Mohite, *Nature* **2016**, *536*, 312.
[5] Z.-K. Tan, R. S. Moghaddam, M. L. Lai, P. Docampo, R. Higler, F. Deschler, M. Price, A. Sadhanala, L. M. Pazos, D. Credgington, F. Hanusch, T. Bein, H. J. Snaith, R. H. Friend, *Nat. Nanotechnol.* **2014**, *9*, 687.
[6] H. Tsai, W. Nie, J.-C. Blancon, C. C. Stoumpos, C. M. M. Soe, J. Yoo, J. Crochet, S. Tretiak, J. Even, A. Sadhanala, G. Azzellino, R. Brenes, P. M. Ajayan, V. Bulović, S. D. Stranks, R. H. Friend, M. G. Kanatzidis, A. D. Mohite, *Adv. Mater.* **2018**, *30*, 1704217.
[7] Y. Zhao, C. Li, L. Shen, *InfoMat* **2019**, *1*, 164.
[8] L. Dou, Y. Yang, J. You, Z. Hong, W.-H. Chang, G. Li, Y. Yang, *Nat. Commun.* **2014**, *5*, 5404.
[9] C. Huang, W. Sun, S. Liu, S. Li, S. Wang, Y. Wang, N. Zhang, H. Fu, S. Xiao, Q. Song, *Laser Photonics Rev.* **2019**, *13*, 1800189.
[10] J. H. Noh, S. H. Im, J. H. Heo, T. N. Mandal, S. I. Seok, *Nano Lett.* **2013**, *13*, 1764.
[11] M. R. Filip, G. E. Eperon, H. J. Snaith, F. Giustino, *Nat. Commun.* **2014**, *5*, 5757.
[12] D. Shi, V. Adinolfi, R. Comin, M. Yuan, E. Alarousu, A. Buin, Y. Chen, S. Hoogland, A. Rothenberger, K. Katsiev, Y. Losovyj, X. Zhang, P. A. Dowben, O. F. Mohammed, E. H. Sargent, O. M. Bakr, *Science* **2015**, *347*, 519.
[13] Q. Dong, Y. Fang, Y. Shao, P. Mulligan, J. Qiu, L. Cao, J. Huang, *Science* **2015**, *347*, 967.
[14] G. Xing, N. Mathews, S. Sun, S. S. Lim, Y. M. Lam, M. Grätzel, S. Mhaisalkar, T. C. Sum, *Science* **2013**, *342*, 344.
[15] A. Owens, A. Peacock, *Nucl. Instrum. Methods Phys. Res., Sect. A* **2004**, *531*, 18.
[16] Y. He, L. Matei, H. J. Jung, K. M. McCall, M. Chen, C. C. Stoumpos, Z. Liu, J. A. Peters, D. Y. Chung, B. W. Wessels, M. R. Wasielewski, V. P. Dravid, A. Burger, M. G. Kanatzidis, *Nat. Commun.* **2018**, *9*, 1609.
[17] H. Wei, Y. Fang, P. Mulligan, W. Chuirazzi, H.-H. Fang, C. Wang, B. R. Ecker, Y. Gao, M. A. Loi, L. Cao, J. Huang, *Nat. Photonics* **2016**, *10*, 333.
[18] Y. He, W. Ke, G. C. B. Alexander, K. M. McCall, D. G. Chica, Z. Liu, I. Hadar, C. C. Stoumpos, B. W. Wessels, M. G. Kanatzidis, *ACS Photonics* **2018**, *5*, 4132.
[19] Y. Dang, D. Ju, L. Wang, X. Tao, *CrystEngComm* **2016**, *18*, 4476.
[20] J. T. Tisdale, T. Smith, J. R. Salasin, M. Ahmadi, N. Johnson, A. V. Ievlev, M. Koehler, C. J. Rawn, E. Lukosi, B. Hu, *CrystEngComm* **2018**, *20*, 7818.
[21] Q. Xu, H. Wei, W. Wei, W. Chuirazzi, D. DeSantis, J. Huang, L. Cao, *Nucl. Instrum. Methods Phys. Res., Sect. A* **2017**, *848*, 106.
[22] Y. He, Z. Liu, K. M. McCall, W. Lin, D. Y. Chung, B. W. Wessels, M. G. Kanatzidis, *Nucl. Instrum. Methods Phys. Res., Sect. A* **2019**, *922*, 217.
[23] S. Yakunin, M. Sytnyk, D. Kriegner, S. Shrestha, M. Richter, G. J. Matt, H. Azimi, C. J. Brabec, J. Stangl, M. V. Kovalenko, W. Heiss, *Nat. Photonics* **2015**, *9*, 444.
[24] L. Li, X. Liu, H. Zhang, B. Zhang, W. Jie, P. J. Sellin, C. Hu, G. Zeng, Y. Xu, *ACS Appl. Mater. Interfaces* **2019**, *11*, 7522.
[25] H. Wei, D. DeSantis, W. Wei, Y. Deng, D. Guo, T. J. Savenije, L. Cao, J. Huang, *Nat. Mater.* **2017**, *16*, 826.
[26] Y. Fang, Q. Dong, Y. Shao, Y. Yuan, J. Huang, *Nat. Photonics* **2015**, *9*, 679.
[27] V. A. Hintermayr, A. F. Richter, F. Ehrat, M. Döblinger, W. Vanderlinden, J. A. Sichert, Y. Tong, L. Polavarapu, J. Feldmann, A. S. Urban, *Adv. Mater.* **2016**, *28*, 9478.
[28] C. Zhang, B. Wang, W. Li, S. Huang, L. Kong, Z. Li, L. Li, *Nat. Commun.* **2017**, *8*, 1138.
[29] N. Rybin, D. Ghosh, J. Tisdale, S. Shrestha, M. Yoho, D. Vo, J. Even, C. Katan, W. Nie, A. J. Neukirch, S. Tretiak, *Chem. Mater.* **2020**, *32*, 1854.
[30] E. Lukosi, T. Smith, J. Tisdale, D. Hamm, C. Seal, B. Hu, M. Ahmadi, *Nucl. Instrum. Methods Phys. Res., Sect. A* **2019**, *927*, 401.
[31] J. T. Tisdale, E. Muckley, M. Ahmadi, T. Smith, C. Seal, E. Lukosi, I. N. Ivanov, B. Hu, *Adv. Mater. Interfaces* **2018**, *5*, 1800476.
[32] J.-W. Lee, S.-G. Kim, J.-M. Yang, Y. Yang, N.-G. Park, *APL Mater.* **2019**, *7*, 041111.
[33] M. De Bastiani, G. Dell'Erba, M. Gandini, V. D'Innocenzo, S. Neutzner, A. R. S. Kandada, G. Grancini, M. Binda, M. Prato, J. M. Ball, M. Caironi, A. Petrozza, *Adv. Energy Mater.* **2016**, *6*, 1501453.
[34] K. Domanski, B. Roose, T. Matsui, M. Saliba, S.-H. Turren-Cruz, J.-P. Correa-Baena, C. R. Carmona, G. Richardson, J. M. Foster, F. De Angelis, J. M. Ball, A. Petrozza, N. Mine, M. K. Nazeeruddin, W. Tress, M. Grätzel, U. Steiner, A. Hagfeldt, A. Abate, *Energy Environ. Sci.* **2017**, *10*, 604.
[35] S. Yakunin, D. N. Dirin, Y. Shynkarenko, V. Morad, I. Cherniukh, O. Nazarenko, D. Kreil, T. Nauser, M. V. Kovalenko, *Nat. Photonics* **2016**, *10*, 585.
[36] Z. Medunić, M. Jakšić, Ž. Pastuović, N. Skukan, *Nucl. Instrum. Methods Phys. Res., Sect. B* **2003**, *210*, 237.
[37] C. Chen, X. Hu, W. Lu, S. Chang, L. Shi, L. Li, H. Zhong, J.-B. Han, *J. Phys. D: Appl. Phys.* **2018**, *51*, 045105.
[38] K.-H. Wang, L.-C. Li, M. Shellaiah, K. Wen Sun, *Sci. Rep.* **2017**, *7*, 13643.
[39] Y. Liu, H. Lu, J. Niu, H. Zhang, S. Lou, C. Gao, Y. Zhan, X. Zhang, Q. Jin, L. Zheng, *AIP Adv.* **2018**, *8*, 095108.
[40] B. Chen, M. Yang, S. Priya, K. Zhu, *J. Phys. Chem. Lett.* **2016**, *7*, 905.
[41] I. Dharmadasa, Y. Rahaq, A. Alam, *J. Mater. Sci.* **2019**, *30*, 12851.
[42] S. A. L. Weber, I. M. Hermes, S.-H. Turren-Cruz, C. Gort, V. W. Bergmann, L. Gilson, A. Hagfeldt, M. Graetzel, W. Tress, R. Berger, *Energy Environ. Sci.* **2018**, *11*, 2404.
[43] H. J. Snaith, A. Abate, J. M. Ball, G. E. Eperon, T. Leijtens, N. K. Noel, S. D. Stranks, J. T.-W. Wang, K. Wojciechowski, W. Zhang, *J. Phys. Chem. Lett.* **2014**, *5*, 1511.
[44] J. Pospisil, A. Guerrero, O. Zmeskal, M. Weiter, J. J. Gallardo, J. Navas, G. Garcia-Belmonte, *Adv. Funct. Mater.* **2019**, *29*, 1900881.
[45] O. Nazarenko, S. Yakunin, V. Morad, I. Cherniukh, M. V. Kovalenko, *NPG Asia Mater.* **2017**, *9*, e373.
[46] M. I. Saidaminov, A. L. Abdelhady, B. Murali, E. Alarousu, V. M. Burlakov, W. Peng, I. Dursun, L. Wang, Y. He, G. Maculan, A. Goriely, T. Wu, O. F. Mohammed, O. M. Bakr, *Nat. Commun.* **2015**, *6*, 7586.